PHYSICS

Final fate of a Leidenfrost droplet: Explosion or takeoff

Sijia Lyu[1]*, Varghese Mathai[2]*, Yujie Wang[1], Benjamin Sobac[3], Pierre Colinet[3], Detlef Lohse[1,4], Chao Sun[1,4]†

When a liquid droplet is placed on a very hot solid, it levitates on its own vapor layer, a phenomenon called the Leidenfrost effect. Although the mechanisms governing the droplet's levitation have been explored, not much is known about the fate of the Leidenfrost droplet. Here we report on the final stages of evaporation of Leidenfrost droplets. While initially small droplets tend to take off, unexpectedly, the initially large ones explode with a crack sound. We interpret these in the context of unavoidable droplet contaminants, which accumulate at the droplet-air interface, resulting in reduced evaporation rate, and contact with the substrate. We validate this hypothesis by introducing controlled amounts of microparticles and reveal a universal 1/3-scaling law for the dimensionless explosion radius versus contaminant fraction. Our findings open up new opportunities for controlling the duration and rate of Leidenfrost heat transfer and propulsion by tuning the droplet's size and contamination.

INTRODUCTION

For a droplet deposited on a heated substrate, the evaporation rate generally increases with the temperature of the substrate. But when the temperature is above a certain value, the droplet levitates on its own vapor layer, and the evaporation rate markedly reduces because of the poor heat conductivity of the vapor layer. This effect, known as the Leidenfrost effect (*1*, *2*), while highly undesirable in certain cooling applications (*3*), can be of great use in many industrial processes, for example, in chemical reactors without borders (*4*), in frictionless transport of small electronic compounds (*5*), in propelling droplets in preferred directions (*6*–*8*), and in drag reduction using the vapor layer (*9*, *10*). As the vapor layer between the levitating droplet and the substrate is of prime importance to the Leidenfrost phenomena, a vast number of studies have been conducted on its characteristics (*2*, *11*–*13*). These have yielded a clear understanding of both the dynamic and quasi-steady aspects of Leidenfrost droplets (*14*, *15*).

However, comparatively little attention has been paid to the final stages of evaporation of Leidenfrost droplets. One of the few investigations is due to Celestini *et al.* (*16*), who conducted experiments with small Leidenfrost droplets of water and ethanol. They reported that when the evaporating droplet becomes smaller than a well-defined radius, it suddenly takes off from the substrate, reaching an elevation much higher than its radius, before it finally disappears. This phenomenon was also observed on substrates below the Leidenfrost temperatures (*17*), where water droplets were found to evaporate down to a critical size and then rapidly rise away. But do all Leidenfrost droplets ultimately take off from the substrate? Here, we study the final stages of evaporation of droplets on very hot substrates. We observe the existence of two final fates for evaporating Leidenfrost droplets: one that leads to droplet explosion and the other resulting in droplet takeoff (*16*). We explain how the physical reason for the two final fates (explosion versus takeoff) lies in the minute amounts of contamination within the droplets, and provide a predictive criterion to determine the final state in terms of the initial conditions of the droplet.

[1]Center for Combustion Energy, Key Laboratory for Thermal Science and Power Engineering of Ministry of Education, Department of Energy and Power Engineering, Tsinghua University, 100084 Beijing, China. [2]School of Engineering, Brown University, Providence, RI 02912, USA. [3]Université libre de Bruxelles, TIPs-Fluid Physics, 1050 Brussels, Belgium. [4]Physics of Fluids Group and Max Planck Center Twente for Complex Fluid Dynamics, University of Twente, Enschede, Netherlands.
*These authors contributed equally to this work.
†Corresponding author. Email: chaosun@tsinghua.edu.cn

RESULTS

The experiments were performed with droplets placed on a heated quartz substrate (see Fig. 1A). Side-view recordings were used to measure the radius, elevation, and state of droplets, while bottom-view images served to distinguish levitation from contact with the substrate. We found two markedly different behaviors at the final evaporation stage (see Fig. 1, B and C), with the same temperature of the substrate (T_s = 296°C). When a "pure" ethanol droplet (pure droplet means a cleanly prepared droplet that meets the analytical reagent standards for purity) of small initial radius, $R_i \approx 30$ μm, is placed on the hot substrate, it first drops down to a lowest location without contacting the substrate and then spontaneously takes off (see Fig. 1B). The lower plot (Fig. 1D) shows the measured levitation height versus time, where the droplet reaches a minimum height $h \approx 50$ μm. In contrast, when the droplet's initial radius is larger, it stably levitates on a vapor layer and finally explodes (see Fig. 1C). A microphone was synchronized with the high-speed camera. In all experiments, the "crack" sound was heard (Fig. 1E) when the explosion occurred, similarly as reported by Leidenfrost (*1*). The same two final fates were observed for a variety of pure liquids, including ultrapure water, ethanol, methanol, butanol, acetone, and hydrofluoroethers (Novec 7000 and Novec 7100 from 3M Ltd.).

From the above observations, it seems that the initial size of the droplet has an important role in the final Leidenfrost dynamics. We hypothesize that the possible reason for the two different final outcomes is the amount of solid contaminants present within the droplet. In general, even with the most careful preparations, no droplet is perfectly pure, but inevitably contains small amounts of contamination. For the pure droplets in our experiments, the volume fraction of contaminants is extremely low [~1 part per million (ppm) (*18*)]. Yet, one can speculate that when a sufficiently large pure droplet evaporates, this small amount of contaminants within the drop can accumulate at the droplet interface, thereby modifying its Leidenfrost dynamics (*19*, *20*).

While one cannot make ethanol purer, an easier route to test our hypothesis is to make the droplet dirtier. We added controlled amounts of hydrophilic rutile titanium dioxide (TiO_2) microparticles into large ethanol droplets (*21*). The particles have a radius $R_p \approx 1$ μm, which is comparable in size to typical contaminants present in pure liquid sample (*18*, *22*). In the experiments, we independently vary the initial amount of particles ϕ_i, the substrate temperature T_s, and the initial droplet radius R_i. The volume fraction ϕ_i is varied by two orders of

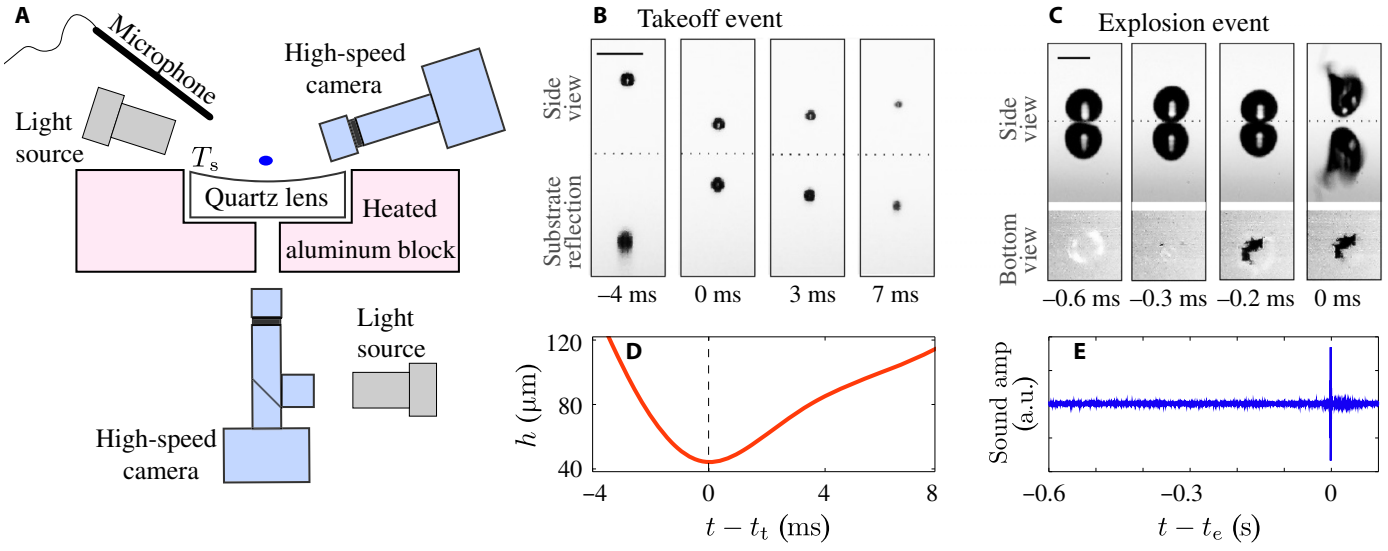

Fig. 1. Experiments showing two different behaviors of evaporating ethanol droplets. (**A**) Experimental setup with two high-speed cameras mounted with long-distance microscopes and a microphone for acquiring the sound signal. (**B** and **C**) Side views of a small (initial radius $R_i \approx 30$ μm; radius in the leftmost image ≈ 17 μm) and a large ethanol droplet (initial radius $R_i = 1.9$ mm; radius in the leftmost image ≈ 53 μm), respectively, in their Leidenfrost states. Scale bars, 100 μm. The temperatures of the substrate are the same, $T_s = 296$°C. The small droplet in (B) remains levitated and eventually takes off; its levitation height versus time $t - t_t$, where t_t is the takeoff time, is shown in (**D**). See also movie S1. The large droplet in (C) remains stably levitated on its vapor layer but finally explodes. The lower row in (C) (bottom-view images) shows the top surface of the substrate at the levitating and exploding stages. A dark patch appears when the droplet is in contact with the substrate. (**E**) Sound signal versus time $t - t_e$ for the large droplet, where t_e is the time of explosion. An audible crack is heard at the time of explosion; see also movie S2 for a recording of the large droplet with sound. Videos of different final fates of Leidenfrost drops are shown in the Supplementary Materials. a.u., arbitrary units.

magnitude, from 10^{-5} up to 10^{-3}. Figure 2A shows the final stages of evaporation of a suspension droplet with an intermediate initial volume fraction ($\phi_i = 10^{-4}$) and the substrate temperature ($T_s = 296$°C). The middle image corresponds to the time when the droplet is at its explosion radius R_e. The droplet had shrunk from its much larger initial radius $R_i = 1.9$ mm (not shown here). On the basis of the radius ratio, we estimate that the droplet is still 90% liquid at this stage. In the immediate following frame, we see that the droplet has undergone a violent explosion, which leads to a marked increase in its lateral size.

We observed that all Leidenfrost droplets with initial size in the range of 1.1 to 2.5 mm and initial concentration in the range of 10^{-5} to 10^{-3} end up exploding at their final stage. Thus, phenomenologically, the final stages of evaporation of suspension droplets seem identical to those of large pure droplets. However, the explosion radius R_e varies for the different cases; while for a suspension droplet R_e can be as large as 0.5 mm, for the pure droplets we observe explosions at $R_e \sim 50$ μm.

DISCUSSION

We develop a model to understand the influence of suspended particles on the droplet explosion radius. For the droplet as shown in Fig. 2A with $R_i = 1.9$ mm, $\phi_i = 10^{-4}$, and $T_s = 296$°C, the typical duration of evaporation $\tau_{dry} \sim 20$ s. The time scale of diffusion $\tau_{mix} \approx R^2/D > 10^3$, where R is the radius of droplets and D is the diffusion coefficient of particles in the liquid. The diffusion time scale $\tau_{mix} \gg \tau_{dry}$, implying that, as the evaporation proceeds, the particles would tend to accumulate and pile up at the droplet-air interface (see Fig. 2B). We also consider the effects of star-shaped oscillation and the inner flow of a droplet. When a droplet shrinks around or smaller than the capillary length scale, we do not observe any star-shaped oscillation, similarly as reported by Ma *et al.* (*23*). Furthermore, Bouillant *et al.* (*24*) recently noted that a single convective roll forms inside the droplet. On the basis of the typical time scale of the roll, the particles Stokes number $St \sim 10^{-5} \ll 1$, and particles may thus be considered nearly tracers (*25*). Hence, the simple rolling flow inside the droplet does not hinder particle accumulation at the interface. This rolling persists until microparticles accumulate and form a static solid shell at the surface (*24*). In addition, Fig. 2C shows one of the pieces of debris remaining after explosion of a droplet. We observed that these shells exist in the debris, similarly as evaporating colloidal droplets (*19*, *26*). We expect the concentration in the shell to approach the random close packing state (*27*), i.e., $\phi_s \approx 0.64$, while we expect that in the bulk of the drop to remain comparable to $\phi_s \sim 10^{-4}$. If the shell thickness scales with the droplet's explosion radius, then mass conservation of the particles results in

$$R_e/R_i \propto \phi_i^{1/3} \quad (1)$$

In Fig. 2D, we plot R_e/R_i versus ϕ_i. The scaling holds remarkably well for the entire range of ϕ_i in our experiments. Further, R_e/R_i is nearly independent of temperature and initial radius, as shown by the insets to Fig. 2D. Using the experimental values of R_i, ϕ_i, and R_e, we estimate the ratio of shell thickness to explosion radius $s^* \approx 0.1 \pm 0.05$. The measured shell thicknesses roughly agree with our expectation of particle accumulation.

We further explore the physical mechanism that triggers the explosions (*28*). Sugiyama *et al.* (*20*) had anticipated that explosions of colloidal-polymer droplets might be triggered by local contact with the substrate, whereas Moreau *et al.* (*29*, *30*) postulated that for surfactant-laden droplets, a buildup of pressure within the droplet

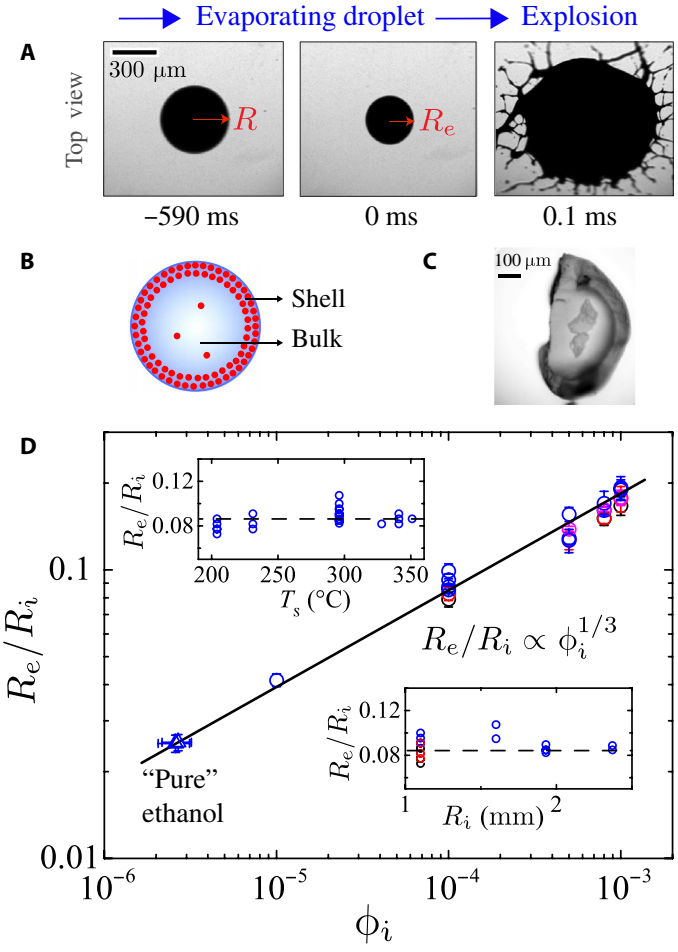

Fig. 2. Explosion details of evaporating Leidenfrost droplets. (**A**) Top view of an evaporating Leidenfrost droplet of ethanol with an initial contaminant volume fraction $\phi_i = 10^{-4}$ and a substrate temperature T_s = 296°C. The middle image shows the droplet at its explosion radius $R_e \approx 150$ μm, after having shrunk from an initial radius R_i = 1.9 mm (not shown here; radius in the leftmost image ≈ 230 μm). The rightmost image shows a violent explosion of the droplet, which leads to a marked increase in its lateral size. (**B**) Schematic of particle accumulation at the receding droplet interface during evaporation, leading to the formation of a shell. (**C**) Picture of an experimental piece of explosion debris with a shell of accumulated particles. Scale bar, 100 μm. (**D**) Ratio R_e/R_i versus ϕ_i for exploding ethanol suspension droplets at various substrate temperatures and for different R_i. The solid line indicates $\phi_i^{1/3}$ scaling. The top inset shows R_e/R_i for a range of substrate temperatures at various initial radii and fixed $\phi_i = 10^{-4}$. The bottom inset shows R_e/R_i for a range of initial droplet radii at various substrate temperatures and fixed $\phi_i = 10^{-4}$. Note that the black, red, blue, and magenta symbols correspond to substrate temperatures 204°, 231°, 296°, and 321°C, respectively, and the triangle symbols in (D) are predictions for pure ethanol droplets based on the observed R_e/R_i and by extrapolating the $\phi_i^{1/3}$ scaling. The error bars represent the SD.

triggers explosion. For our suspension droplets, we look more closely into the events leading up to the explosion (see Fig. 3A). In the first image, the droplet is in a stably levitated state, as revealed by the side and bottom views. In the second image at $\tilde{t} = -0.1$ ms, the bottom view indicates local contact with the substrate. This can trigger sudden boiling at the contact point and lead to the explosion seen in the rightmost image. An almost identical local contact triggers the explosion for the other droplets studied, as well as for pure droplets (see Fig. 1C, bottom row).

While it has become clear that local contact occurs before the explosion, it remains to be explained what causes the stably levitated drop (Fig. 3A, leftmost image) to suddenly touch down on the substrate. Below, we model the vapor flow that levitates the evaporating Leidenfrost droplet. When the size is much smaller than the capillary length ℓ_c ($\ell_c \approx 1.5$ mm for ethanol), the droplet may be expected to become nearly spherical. The bottom surface of the droplet is nearly flat (*12*, *31*), with the horizontal extent (*32*) $l \approx R^2/\ell_c$ much smaller than the droplet radius (*12*, *13*), and the temperature inside the droplet is nearly homogeneous (*12*, *24*). For these droplets, the evaporation rate can be expected to be nearly uniform at the interface (*12*). Consequently, the volume flow rate of vapor per unit area is given by

$$\dot{q} = \frac{\rho_l}{4\pi R^2 \rho_v}\left|\frac{dQ}{dt}\right| \quad (2)$$

where ρ_v and ρ_l are the vapor and liquid densities, respectively, and $|dQ/dt|$ is the rate of volume change of the droplet, which can be calculated from images of the evaporating droplet. Continuous evaporation between the droplet's base and the substrate leads to an escaping thin layer of vapor, which exerts a high pressure on the drop. Assuming that the vapor layer is in a quasi-steady state, the evaporation flux of the flat region is equal to the radial flow flux in the vapor layer (see Fig. 3B, inset), giving

$$v_r(r) = \frac{\dot{q}r}{2h} \quad (3)$$

Here, $v_r(r)$ is the horizontal radial velocity in the vapor layer at a distance r from the center of the flat region, and h is the thickness of the vapor layer. Because the vapor layer thickness and its variation are very small as compared to its horizontal extent (*12*, *13*, *31*, *33*), h can be assumed to be independent of r (*12*, *31*). In this limit, the lubrication approximation can be used, which leads to a lift force (*31*)

$$F_v = 12\pi\mu_v \int_o^l \frac{v_r r^2}{h^2} dr \quad (4)$$

where μ_v is the dynamic viscosity of the vapor. Under the condition of stable levitation, the lift force balances the droplet's weight containing particles in suspension $G = [\rho_p Q_p + \rho_l(Q - Q_p)]g$, where ρ_p is the density of particles, Q_p is the volume of particles, and g is the gravitational acceleration. Integrating Eq. 4 and equating to G, we obtain an expression for the evolving thickness of the vapor layer

$$h \approx \left(\frac{3}{8}\frac{\mu_v \rho_l R^6}{\rho_v G \ell_c^4}\left|\frac{dQ}{dt}\right|\right)^{1/3} \quad (5)$$

Figure 3B shows the calculated vapor layer thickness h versus the time to explosion $t - t_e$, where t_e is the explosion time. The liquid with particles can still evaporate, although the thickness of the vapor layer decreases as time. When the particles have accumulated to such an extent that the liquid at the interface is not enough to fill around the particles, the roughness length scale of the droplet interface becomes comparable to the particle size. As evident from Fig. 3B, when h approaches around this critical thickness, the droplet locally contacts the heated substrate, thereby triggering the explosion. The same

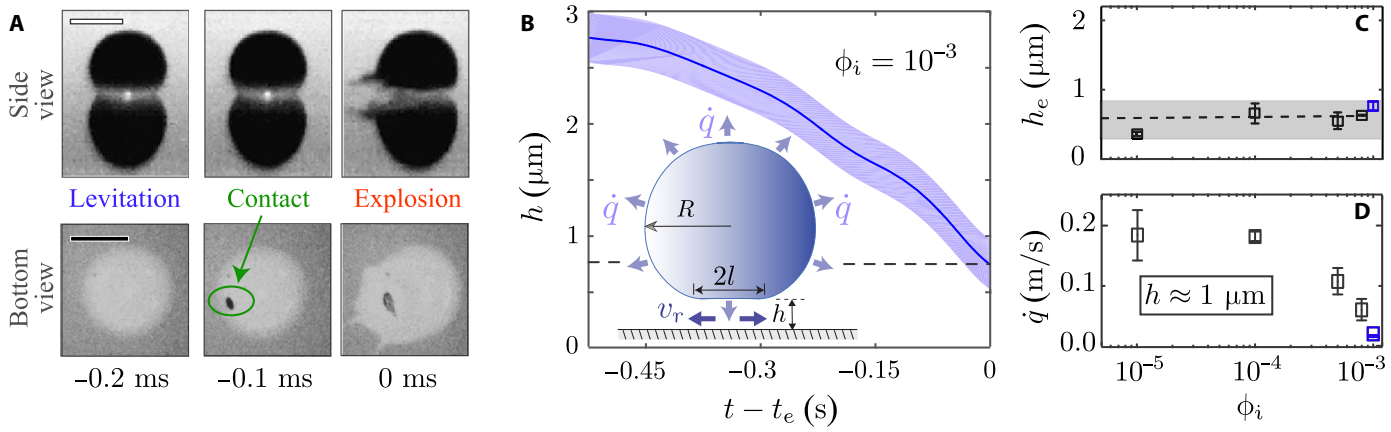

Fig. 3. Local contact and explosion modeling of evaporating Leidenfrost droplets. (**A**) Side and bottom views of a suspension droplet just before and at the point of explosion; here, R_i = 1.6 mm, $\phi_i = 10^{-4}$, and T_s = 296°C. Scale bars, 200 μm. (**B**) Vapor layer thickness h versus time to explosion $t - t_e$ for an evaporating drop, where h was estimated using Eq. 5. We find that the explosion occurs when h approaches 1 μm, which is comparable to the particle size. The inset shows a schematic of the levitation model used in the estimation of h. (**C**) Thickness h_e of the vapor layer (calculated) at explosion, for droplets with ϕ_i varying from 10^{-5} to 10^{-3}. Note that h_e stays nearly constant (~1 μm), i.e., comparable to the particle size. (**D**) Surface averaged volume flow rate, $\dot{q}$, when the vapor layer is 1 μm thick. Note that $\dot{q}$ decreases with ϕ_i, suggesting that the accumulation of the particles at the droplet interface inhibits evaporation. The error bars represent the range of the data.

holds for other initial concentrations ϕ_i. Figure 3C shows that the vapor layer thickness at explosion h_e is around 1 μm for all volume fractions tested. At this stage, the evaporation may be limited by the liquid flow through the porous shell formed on the droplet's surface. Because the shell formed is thicker for the larger ϕ_i cases, $\dot{q}$ decreases with increasing ϕ_i (see Fig. 3D).

How can the explosion of suspension droplets be insightful to pure liquid droplets? First, the images of exploding pure liquid droplets are similar to those of suspension droplets (see Figs. 1C and 3A). Furthermore, for the pure droplets of various initial radii tested, we found that the dimensionless explosion radius remains constant ($R_e/R_i \approx 0.25 \pm 0.002$). We extrapolate the scaling dependence between R_e/R_i and ϕ_i to pure ethanol (see triangle symbols in Fig. 2D). This yields a prediction of $\phi_i \approx 2 \times 10^{-6}$, which is a good estimate of the contamination levels in analytical reagent of ethanol.

Because R_e/R_i is independent of the initial radius (Fig. 2D, bottom inset), we can say that as the initial droplet size reduces, the explosion radius also becomes smaller. However, at some critical initial radius R_{ic}, the droplet size R approaches the thickness of the vapor layer h. In this limit, the lubrication model (in Eq. 4) will no longer be valid, and the droplet then enters the takeoff regime (in this regime, the convective heat flux is negligible compared to the diffusive flux) and spontaneously rises away (*16*, *17*). In this regime, Celestini *et al.* (*16*) balanced the drag force and the weight of the droplet and derived a scaling law relating the droplet's elevation to its radius: $h/R \propto R^{-3/2}$. We measured the dimensionless elevation height h/R of ethanol droplets as a function of the radius R during the evaporation from the experiment using the high-speed images (see Fig. 1B) and find a good agreement between our data and the −3/2 scaling law (see Fig. 4A). We define the maximal radius that satisfies this scaling relation as the takeoff radius R_t for pure droplets and, similarly, for suspension droplets. After the droplet has shrunk to R_t, it stays in a quasi-static state and steadily rises as the evaporation proceeds. We found that for pure and suspension droplets of ethanol, R_t lies in the range 15 ± 1 μm, which is much larger than these small droplets' predicted explosion radii. Thus, an evaporating small droplet reaches the takeoff radius well before its explosion radius. At this stage, the shell, which causes the reduced evaporation and the resulting contact with the substrate, has not yet formed. Hence, the small droplet rises up above the substrate and escapes its explosion fate.

Comparing the explosion radius R_e and the takeoff radius R_t, we find that a large droplet ($R_e > R_t$) first shrinks to the explosion radius, contacts the substrate, and explodes, while a small droplet ($R_t > R_e$) shrinks to the takeoff radius and rises away from the substrate. While R_e strongly depends on the initial conditions of the droplet, we found that the takeoff radius, $R_t \approx 14$ to 16 μm, is only weakly affected by initial size and contamination levels. Therefore, we can use $R_e = R_t$ as a criterion to calculate the critical (or transitional) initial radius, R_{ic}, that separates the takeoff regime from the explosion regime. Figure 4B shows a prediction of R_{ic} as applied to pure and suspension droplets with varying levels of contamination ϕ_i, at $T_s \approx 300$°C. For a droplet of perfectly pure liquid ($\phi_i = 0$), there should be no explosion, regardless of the droplet's initial size, because $R_{ic} \to \infty$ for $\phi_i = 0$. However, in practice for pure droplets with unavoidable contaminations ($\phi_i \sim 2 \times 10^{-6}$), $R_{ic} \approx 0.6$ mm. With increasing contamination, R_{ic} decreases, until it reaches about 100 μm at $\phi_i = 10^{-3}$. In this situation, explosion becomes the likely fate of evaporating Leidenfrost droplets. Note that the R_{ic} versus ϕ_i prediction in Fig. 4B was obtained using the takeoff radius $R_t = 15 \pm 1$ μm we observed for pure and "suspension" droplets. Although the particles do not seem to affect the value of R_t, their effect will become prominent at high particle concentrations. This deserves further studies in the future.

CONCLUSION

In summary, we have shown that both initial size and level of contamination determine the fate of Leidenfrost droplets. Large droplets explode and small droplets take off at the final Leidenfrost stage. The dimensionless explosion radius has a 1/3 power-law dependence on the initial volume fraction of particles ϕ_i. The explosion is caused by contaminants, which accumulate at the interface as the droplet evaporates and concurrently decrease the evaporation rate. When the vapor layer thickness approaches the contaminant microparticle radius, the droplet locally contacts the hot substrate and explodes. In this situation, the contaminant particles could act as a nucleus for the sudden boiling event. Furthermore, it is also plausible that

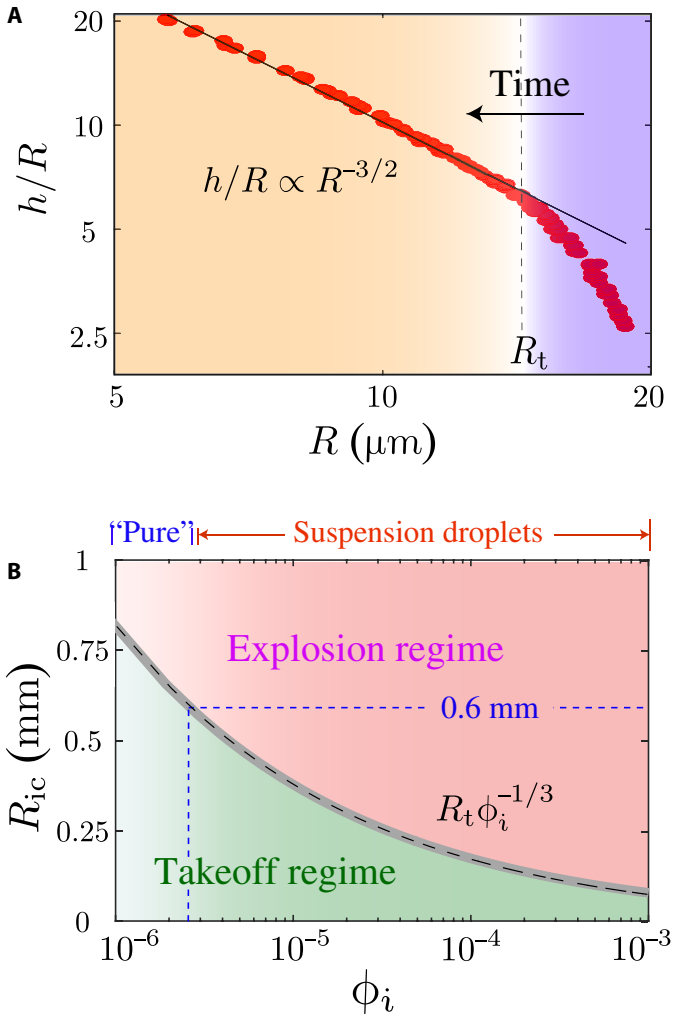

Fig. 4. Predictions of takeoff and explosion regimes for pure and suspension droplets of ethanol. (**A**) Dimensionless elevation h/R of a small pure ethanol droplet as a function of its radius R, as measured from experiment by using the high-speed images, at $T_s = 296$°C. At a takeoff radius $R_t \approx 15$ μm (vertical dashed line), the shrinking droplet enters a quasi-static regime and follows the scaling $h/R \propto R^{-3/2}$. (**B**) Predicted critical initial radius R_{ic} versus contamination level ϕ_i for $T_s = 296$°C. This R_{ic} separates the explosion regime from the takeoff regime. For pure ethanol drop ($\phi_i \approx 2 \times 10^{-6}$), $R_{ic} \approx 0.6$ mm. With increasing contamination ϕ_i, R_{ic} decreases, which makes explosion the more likely outcome.

the local contact is aided by the gravitational settling of clumped TiO_2 particles; however, this deserves further study in future. We observed the same two final fates for a variety of pure liquids (laboratory grade; nonvolatile residue, ~1 ppm), including ultrapure water, ethanol, methanol, butanol, acetone, and hydrofluoroethers (Novec 7000 and Novec 7100). Therefore, one can conclude that the two regimes witnessed here are general to the fate of evaporating Leidenfrost droplets—the initial size of droplet has a major influence on its final fate.

The present research has also solved the mystery of the audible crack heard by Leidenfrost (*1*) in 1756 and, at the same time, provided a unified understanding of the final stage of Leidenfrost dynamics applicable to pure and suspension droplets, bridging nearly three orders of magnitude variation in initial concentration. These insights could help develop novel strategies for controlled particle transport and deposition using the Leidenfrost effect. For instance, Leidenfrost droplets could serve as carriers of microcomponents in electronics (*6*), wherein their transport and deposition can be controlled by tuning droplet size and particle concentration. Other avenues could lie in heat transfer enhancement, wherein the addition of impurities can trigger the early loss of Leidenfrost state. Last, the robust radius ratio versus particle concentration scaling we uncovered here opens up the possibility of developing new techniques to assess the purity of liquid samples.

MATERIALS AND METHODS

Experimental methods

The experiments had to be performed in a very clean environment. The following procedure was adopted for cleaning the needle, quartz substrate, and spray nozzle used in the experiments. Before each experiment, the components were immersed in acetone and placed in an ultrasonic bath for 2 min. The same procedure was repeated with ethanol and finally using ultrapure water. After this, purified compressed air was blown to dry the components. An air purifier in the laboratory ensured a clean environment during the experiment.

The experiments were performed using a variety of liquids including ultrapure water, ethanol, methanol, butanol, acetone, and hydrofluoroethers (Novec 7000 and Novec 7100 from 3M Ltd.). The droplets were deposited on a slightly curved quartz substrate. The top surface of the substrate has a curvature radius of 114.5 mm, allowing us to keep droplets in the camera field of view (see Fig. 1A). The substrate was placed on a heated aluminum block controlled by a PID (proportional, integral, derivative) controller. The surface temperature T_s of the substrate was measured with a thermocouple that was stuck to the substrate. Two sets of high-speed cameras with long-distance microscopes were used to record the evaporation process from the side and below simultaneously. The side-view recordings were used to measure the radius, elevation, and state of droplets, while the bottom-view images served to distinguish levitation from contact with the substrate. When a vapor layer exists, the strong reflected light results in a bright spot around the base of the droplet. When the droplet contacts the substrate, the wetted area is seen as a dark patch (*15*, *33*, *34*).

A spray generator was used to produce small ethanol droplets. The initial size of droplets R_i was in the range of 19 to 52 μm, and the average size was about 30 μm. A board with an opening was placed between the spray and the substrate to reduce the number of droplets falling in the observation area. Larger droplets with R_i larger than 0.9 mm were created using a microliter pipette. Figure 1 (B and C) compares the Leidenfrost dynamics of two droplets of very different initial radii.

Preparation of the suspension

The amount of hydrophilic rutile titanium dioxide (TiO_2) microparticles (from Macklin) to be added was weighed using an electronic balance. For particles, the radius R_p is about 1 μm and the purity is about 99%. Controlled quantities were added to laboratory-grade ethanol for obtaining different particle concentrations. Ethanol was chosen for the experiments because its low surface tension limits the amount of contaminants within the droplets and its low latent heat enables a high evaporation rate. The different concentrations of suspensions were stored in airtight bottles. To avoid the deposition of the microparticles, before each sampling, the bottles were immersed in the ultrasonic bath, and then the suspension was shaken vigorously with a vortex shaker

from Kylin-Bell (product number: VORTEX-5). To further avoid the possibility of particles segregating, the syringe used for the experiment was also shaken before each experiment.

Image processing

The boundary of the droplet was identified using MATLAB, and a circle fitting function (*35*) was used to obtain the radius of the droplet R and the position of the center of the droplet. For the explosion regime, the droplet radius R was used to estimate the volume of the sphere droplet $Q = \frac{4}{3}\pi R^3$. Then, we used Eq. 5 to calculate the thickness of the vapor layer. When the radius of the droplet suddenly increases sharply, it indicates that the droplet has exploded, and R_e was defined as the radius just before explosion. For the large droplets created by the microliter pipette, we used a set volume to calculate the initial radius of the droplet R_i.

For the takeoff regime, we used the high-speed images to get the elevation of the droplet. The central axis between the droplet and its mirror image is the position of the plate. The distance between the droplet center and the plate is z, and the distance between the bottom surface of the droplet and the plate is $h = z - R$. For small spray droplets, we recorded the images near the spray nozzle and used image processing to calculate the initial size range.

SUPPLEMENTARY MATERIALS

Supplementary material for this article is available at http://advances.sciencemag.org/cgi/content/full/5/5/eaav8081/DC1

Movie S1. The small pure ethanol droplet remains levitated and eventually takes off on a heated substrate.

Movie S2. The large pure ethanol droplet on a heated substrate remains stably levitated on its vapor layer but finally explodes with a crack sound.

REFERENCES AND NOTES

1. J. G. Leidenfrost, *De Aquae Communis Nonnullis Qualitatibus Tractatus* (Ovenius, 1756).
2. D. Quéré, Leidenfrost dynamics. *Annu. Rev. Fluid Mech.* **45**, 197–215 (2013).
3. V. Dhir, Boiling heat transfer. *Annu. Rev. Fluid Mech.* **30**, 365–401 (1998).
4. M. Elbahri, D. Paretkar, K. Hirmas, S. Jebril, R. Adelung, Anti-lotus effect for nanostructuring at the Leidenfrost temperature. *Adv. Mater.* **19**, 1262–1266 (2007).
5. A. Hashmi, Y. Xu, B. Coder, P. A. Osborne, J. Spafford, G. E. Michael, G. Yu, J. Xu, Leidenfrost levitation: Beyond droplets. *Sci. Rep.* **2**, 797 (2012).
6. G. Lagubeau, M. Le Merrer, C. Clanet, D. Quéré, Leidenfrost on a ratchet. *Nat. Phys.* **7**, 395–398 (2011).
7. H. Linke, B. J. Alemán, L. D. Melling, M. J. Taormina, M. J. Francis, C. C. Dow-Hygelund, V. Narayanan, R. P. Taylor, A. Stout, Self-propelled Leidenfrost droplets. *Phys. Rev. Lett.* **96**, 154502 (2006).
8. B. Sobac, A. Rednikov, S. Dorbolo, P. Colinet, Self-propelled Leidenfrost drops on a thermal gradient: A theoretical study. *Phys. Fluids* **29**, 082101 (2017).
9. I. U. Vakarelski, N. A. Patankar, J. O. Marston, D. Y. C. Chan, S. T. Thoroddsen, Stabilization of Leidenfrost vapour layer by textured superhydrophobic surfaces. *Nature* **489**, 274–277 (2012).
10. I. U. Vakarelski, J. D. Berry, D. Y. C. Chan, S. T. Thoroddsen, Leidenfrost vapor layers reduce drag without the crisis in high viscosity liquids. *Phys. Rev. Lett.* **117**, 114503 (2016).
11. J. H. Snoeijer, P. Brunet, J. Eggers, Maximum size of drops levitated by an air cushion. *Phys. Rev. E* **79**, 036307 (2009).
12. A.-L. Biance, C. Clanet, D. Quéré, Leidenfrost drops. *Phys. Fluids* **15**, 1632–1637 (2003).
13. J. C. Burton, A. L. Sharpe, R. C. A. van der Veen, A. Franco, S. R. Nagel, Geometry of the vapor layer under a Leidenfrost drop. *Phys. Rev. Lett.* **109**, 074301 (2012).
14. B. Sobac, A. Rednikov, S. Dorbolo, P. Colinet, Leidenfrost effect: Accurate drop shape modeling and refined scaling laws. *Phys. Rev. E* **90**, 053011 (2014).
15. M. Shirota, M. A. J. van Limbeek, C. Sun, A. Prosperetti, D. Lohse, Dynamic Leidenfrost effect: Relevant time and length scales. *Phys. Rev. Lett.* **116**, 064501 (2016).
16. F. Celestini, T. Frisch, Y. Pomeau, Take off of small Leidenfrost droplets. *Phys. Rev. Lett.* **109**, 034501 (2012).
17. D. V. Zaitsev, D. P. Kirichenko, V. S. Ajaev, O. A. Kabov, Levitation and self-organization of liquid microdroplets over dry heated substrates. *Phys. Rev. Lett.* **119**, 094503 (2017).
18. E. Oberdörster, Manufactured nanomaterials (fullerenes, C_{60}) induce oxidative stress in the brain of juvenile largemouth bass. *Environ. Health Perspect.* **112**, 1058–1062 (2004).
19. N. Tsapis, E. R. Dufresne, S. S. Sinha, C. S. Riera, J. W. Hutchinson, L. Mahadevan, D. A. Weitz, Onset of buckling in drying droplets of colloidal suspensions. *Phys. Rev. Lett.* **94**, 018302 (2005).
20. Y. Sugiyama, R. J. Larsen, J.-W. Kim, D. A. Weitz, Buckling and crumpling of drying droplets of colloid-polymer suspensions. *Langmuir* **22**, 6024–6030 (2006).
21. M. Osękowska, E. Karuga-Kuźniewska, D. Wojcieszak, M. Mazur, A. Poniedzialek, D. Kaczmarek, M. Szymonowicz, Z. Rybak, Influence of nanocrystalline structure and surface properties of TiO_2 thin films on the viability of L929 cells. *Pol. J. Chem. Technol.* **17**, 33–39 (2015).
22. K. He, F. Yang, Y. Ma, Q. Zhang, X. Yao, C. K. Chan, S. Cadle, T. Chan, P. Mulawa, The characteristics of $PM_{2.5}$ in Beijing, China. *Atmos. Environ.* **35**, 4959–4970 (2001).
23. X. Ma, J.-J. Liétor-Santos, J. C. Burton, Star-shaped oscillations of Leidenfrost drops. *Phys. Rev. Fluids* **2**, 031602 (2017).
24. A. Bouillant, T. Mouterde, P. Bourrianne, A. Lagarde, C. Clanet, D. Quéré, Leidenfrost wheels. *Nat. Phys.* **14**, 1188–1192 (2018).
25. V. Mathai, E. Calzavarini, J. Brons, C. Sun, D. Lohse, Microbubbles and microparticles are not faithful tracers of turbulent acceleration. *Phys. Rev. Lett.* **117**, 024501 (2016).
26. T. Okuzono, K. Ozawa, M. Doi, Simple model of skin formation caused by solvent evaporation in polymer solutions. *Phys. Rev. Lett.* **97**, 136103 (2006).
27. G. Scott, D. M. Kilgour, The density of random close packing of spheres. *J. Phys. D Appl. Phys.* **2**, 863 (1969).
28. N. Zhang, W.-J. Yang, Evaporation and explosion of liquid drops on a heated surface. *Exp. Fluids* **1**, 101–111 (1983).
29. F. Moreau, P. Colinet, S. Dorbolo, Leidenfrost explosions. *Phys. Fluids* **25**, 091111 (2013).
30. F. Moreau, P. Colinet, S. Dorbolo, Explosive Leidenfrost droplets. *Phys. Rev. Fluids* **4**, 013602 (2019).
31. H. Y. Lo, Y. Liu, L. Xu, Mechanism of contact between a droplet and an atomically smooth substrate. *Phys. Rev. X* **7**, 021036 (2017).
32. L. Mahadevan, Y. Pomeau, Rolling droplets. *Phys. Fluids* **11**, 2449–2453 (1999).
33. R. C. A. van der Veen, T. Tran, D. Lohse, C. Sun, Direct measurements of air layer profiles under impacting droplets using high-speed color interferometry. *Phys. Rev. E* **85**, 026315 (2012).
34. J. M. Kolinski, S. M. Rubinstein, S. Mandre, M. P. Brenner, D. A. Weitz, L. Mahadevan, Skating on a film of air: Drops impacting on a surface. *Phys. Rev. Lett.* **108**, 074503 (2012).
35. V. Mathai, V. N. Prakash, J. Brons, C. Sun, D. Lohse, Wake-driven dynamics of finite-sized buoyant spheres in turbulence. *Phys. Rev. Lett.* **115**, 124501 (2015).

Acknowledgments: We thank E. Guo and A. Xia for their help with experiments. We acknowledge S. Dorbolo, C. D. Ohl, H. A. Stone, H. Xu, and X. Chao for fruitful discussions. We are also grateful to two anonymous referees for their insightful suggestions. **Funding:** This work was financially supported by the Natural Science Foundation of China (grants 91852202, 11672156, and 11861131005), the Netherlands Organisation for Scientific Research (NWO), and the Fonds de la Recherche Scientifique (F.N.R.S.) (postdoctoral researcher position of B.S. and research director position of P.C.). **Author contributions:** C.S., S.L., and V.M. designed the research. S.L., Y.W., and V.M. performed the experiments. S.L., V.M., and B.S. performed the analyses and discussed the results with P.C., D.L., and C.S. V.M., S.L., and C.S. drafted the manuscript, and D.L., B.S., and P.C. contributed to the revisions of the manuscript. **Competing interests:** The authors declare that they have no competing interests. **Data and materials availability:** All data needed to evaluate the conclusions in the paper are present in the paper and/or the Supplementary Materials. Additional data related to this paper may be requested from the authors. Correspondence and requests for materials should be addressed to C.S. (chaosun@tsinghua.edu.cn).

Submitted 22 October 2018
Accepted 15 March 2019
Published 3 May 2019
10.1126/sciadv.aav8081

Citation: S. Lyu, V. Mathai, Y. Wang, B. Sobac, P. Colinet, D. Lohse, C. Sun, Final fate of a Leidenfrost droplet: Explosion or takeoff. *Sci. Adv.* **5**, eaav8081 (2019).

Final fate of a Leidenfrost droplet: Explosion or takeoff

Sijia Lyu, Varghese Mathai, Yujie Wang, Benjamin Sobac, Pierre Colinet, Detlef Lohse and Chao Sun

Sci Adv **5** (5), eaav8081.
DOI: 10.1126/sciadv.aav8081